

Broadband ground-motion modeling and shaking scenarios for the 2009 L'Aquila (Central Italy) earthquake

G. Ameri, & F. Pacor

Istituto Nazionale di Geofisica e Vulcanologia, Milan, Italy

F. Gallovič

Charles University, Prague, Czech Republic



SUMMARY

The 6 April 2009 (M_w 6.3) L'Aquila, central Italy, earthquake has been recorded by relatively large number of digital strong-motion stations. We model the strong-motion records of the L'Aquila earthquake over the entire frequency band of engineering concern (0.1 - 10 Hz), using a hybrid integral-composite approach based on a k-square kinematic rupture model, combining low-frequency coherent and high-frequency incoherent source radiation.

The synthetic seismograms show a good agreement with observed waveforms both in terms of acceleration and velocity. The fit is judged according to an objective goodness-of-fit criteria, that give, on average, from fair to very good scores. The validated model has been then used to simulate ground-motion maps in the study area for bedrock site condition. Finally, the simulated ground motions in the epicentral area have been compared with European and Italian ground motion prediction equations GMPEs.

Keywords: Broadband simulations, 2009 L'Aquila earthquake, shaking scenarios, goodness-of-fit,

1. INTRODUCTION

On April 6, 2009, at 1:32 GMT, a M_w 6.3 earthquake struck L'Aquila city, one of the largest urban centers in the Abruzzo region (central Italy) with about 70,000 inhabitants, causing 308 casualties and vast destruction in the town and surrounding villages. This event represents the third largest earthquake recorded by strong-motion instruments in Italy, after the 1980, M_w 6.9, Irpinia and the 1976, M_w 6.4, Friuli earthquakes.

The earthquake occurred along a NW-SE trending normal fault, approximately 20 km long, dipping about 45° SW. The hypocenter depth was estimated at 9.5 km, and the epicenter at less than 5 km SW of the town center (Chiarabba et al., 2009).

The earthquake has been recorded by relatively large number of digital strong-motion stations. Such a dataset is unique in Italy in terms of number and quality of records, azimuthal coverage and presence of near-fault recordings (Ameri et al., 2009). A number of studies on low-frequency source inversion showed that the rupture followed a complex pattern with a slip distribution composed by at least two asperities and a variable rupture velocity over the fault plane possibly including a temporal rupture stop (e.g., Cirella et al., 2009; Gallovič and Zahradník, 2012).

In this paper we present an overview of the modeling of the strong-motion records from the L'Aquila earthquake over the entire frequency band of engineering concern (0.1 - 10 Hz). The synthetic seismograms at the recorded stations are validated through a goodness-of-fit analysis that includes relevant engineering metrics. Then, we simulate the ground motion at a dense number of virtual stations in the epicentral area, discuss the ground motion distribution and compare the predicted peak acceleration and velocity values with empirical ground motion prediction equations (GMPEs).

2. DATA AND MODELS

The L'Aquila earthquake was recorded by 56 digital strong-motion stations (Ameri et al., 2009) belonging to the national strong-motion network (RAN). All the records are available in the Italian Accelerometric Archive (ITACA <http://itaca.mi.ingv.it/>). The epicentral distances range from 1.7 km to about 276 km with Joyner-Boore distances (R_{JB}) ranging from 0 to 266 km. In particular, there are 17 records with R_{JB} smaller than 50 km and five records with $R_{JB} = 0$ (Fig. 1 and Tab. 1). Three of these $R_{JB} = 0$ stations are part of an array deployed in the upper Aterno-river valley (AQG, AQA and AQV) whereas the other two (i.e., AQK and AQU) are in downtown L'Aquila. In the following we will refer to this group of near-fault stations simply as "AQ_". The largest PGA and PGV are 646 cm/s^2 and 43 cm/s , respectively, recorded at station AQV.

In Table 1, the sites are classified according to the Eurocode 8 (EC8; CEN, 2004) and the Italian Building Code (NTC08, 2008), based on the shear-wave velocity averaged over the top 30 m of the soil profile - $V_{s,30}$. The class of each station has been attributed on the basis of direct measure of $V_{s,30}$ or on geological/geophysical information (S4 project-Deliverable D4, 2009; <http://esse4.mi.ingv.it>; Di Capua et al., 2011).

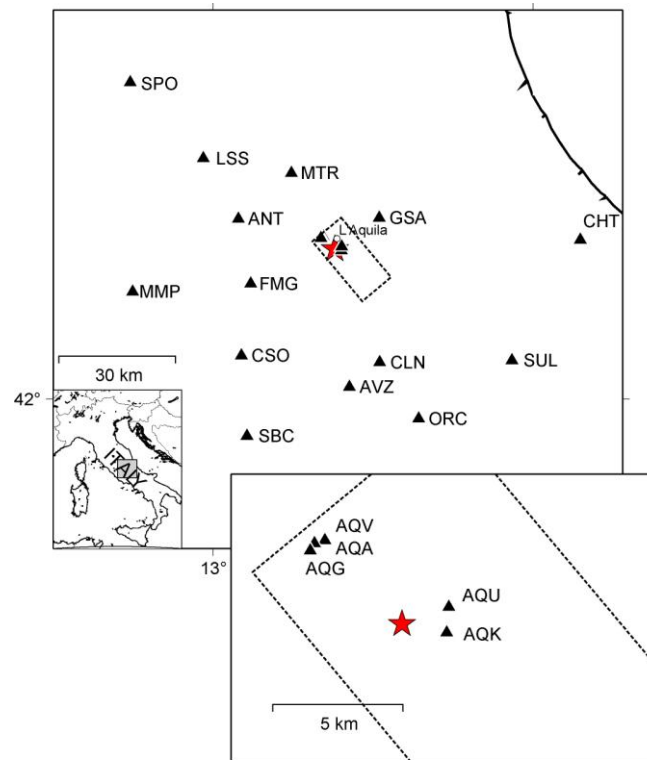


Figure 1. Map showing the epicentral area of the 6 April 2009 L'Aquila earthquake. The strong motion stations are marked by triangles (see also Tab. 1). The inset shows a zoom on the near-fault (AQ_) stations. The earthquake epicenter and the surface projection of the rupture plane are indicated by the red star and the dashed rectangle, respectively.

For the strong ground-motion modeling we use hybrid integral-composite (HIC) approach introduced by Gallovič and Brokešová (2007). This model is designed mostly for the earthquake ground-motion simulations, providing omega-squared source spectrum. The HIC technique simulates the rupture process in terms of slipping of elementary subsources with fractal number-size distribution (fractal dimension 2), randomly placed on the fault plane, with the exception of the largest subsources that can be placed to mimic slip asperities positions. At low frequencies, the source description is based on the representation theorem (integral approach), assuming a final slip distribution composed from the subsources, which is characterized by a k-squared decay (Herrero and Bernard, 1994). At high frequency, instead, the ground-motion synthesis is obtained summing the contributions from each

individual subsurface treated as a point source (composite approach). The integral and composite calculations are crossover combined in the frequency domain to obtain broadband seismograms. In this study, we use a variable crossover frequency band for near and far stations from the source (see Ameri et al., 2012).

In the following we briefly describe the source and wave propagation models and we refer to Ameri et al. (2012) for further and more detailed information.

We use a rectangular fault plane 20 km long and 15 km wide having a strike of 140° and dipping 50° toward south-west. The rake angle is -90° (pure normal-fault mechanism) and the hypocentral depth is 9 km. We constrain the basic features of the kinematic rupture model according to the low-frequency inversion (< 0.2 Hz) performed by Galovic and Zahradnik (2012). The final HIC source model is characterized by a rupture time distribution obtained assuming two rupture velocities and a nucleation point corresponding to the instrumental hypocenter. As suggested by the slip inversion, a rupture delay of the southern asperity by approximately 3s is also included in the model. We test different rupture velocities and set the final values in the bottom and top part of the fault equal to $V_r=3$ km/s and $V_r=2$ km/s, respectively. A sketch of the source model is shown in Fig. 2.

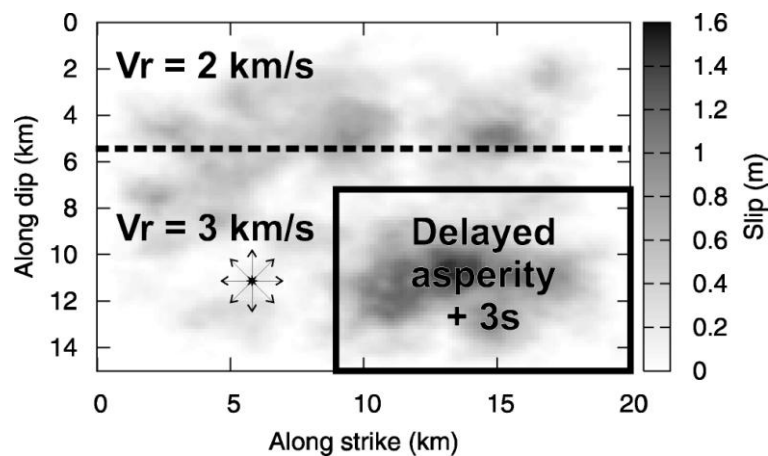


Figure 2. Kinematic rupture model used in the simulations. The final k-squared slip distribution composed of slip contributions from the fractal subsources is mapped by gray tones. The rupture velocity (V_r) values used in the top and bottom part of the fault as well as the location of the delayed asperity are illustrated. The outward vectors indicate the rupture nucleation point.

The final slip distribution is obtained constraining the positions of the three largest subsources, that are characterized by the largest seismic moment, according to Galovic and Zahradnik (2012). In particular, one of them is placed “above” the hypocenter and the other two are set in the southern bottom part of the fault. At small scale, 60 subsources are randomly distributed over the fault plane following the defined number-size distribution, composing random high-wavenumbers details of the slip distribution.

Finally, the stress drop of the whole event is set to 100 bars based on estimates by Bindi et al. (2009) and on comparison between observed and synthetic high-frequency level of the Fourier amplitude spectra.

The Green’s functions for both calculations are calculated by the discrete wave-number technique, DWN (Bouchon, 1981), either in general 1D layered model or in specific 1D models for the individual stations that include low-velocity subsurface layers, where available. The DWN technique provides full wave-field Green’s functions; no stochastic Green’s functions are used. In particular we use the 1D velocity model proposed by Bianchi et al. (2010), characterized by 6 horizontal layers down to 42 km having a shear velocity at surface equal to 1700 m/s. Beside the regional wave propagation characteristics we need to account, in the simulated seismograms, for the effect of amplification (or de-amplification) of seismic waves occurring in the shallow-most soil layers (i.e., in the last tens of meters). We opt for incorporation of site response only by including site-specific 1D soil layers in the crustal model; for five of the closest stations to the epicenter (AQA, AQV, AQG, GSA and AVZ) such 1D profiles are available (<http://itaca.mi.ingv.it>). For the remaining stations, the synthetics are

computed using the general 1D crustal model without including site-specific effects (see Ameri et al., 2012 for further details).

To properly describe the high-frequency spectral decay of synthetics, we adopt the κ operator, introduced by Anderson and Hough (1984). We set $\kappa= 0.03s$, that is a typical value for rock sites in Italy (Bindi et al., 2004).

3. MODELING RESULTS AND VALIDATION

Fig. 3 presents an overview of the modeling results, showing comparison of synthetic and observed acceleration and velocity time histories and acceleration response spectra for 11 selected stations (Tab. 1 and Fig. 1).

The fit is judged according to the goodness-of-fit (GOF) criteria defined by Olsen and Mayhew (2010). They proposed a GOF algorithm based on different metrics, among which we selected: Peak Ground Acceleration (PGA), velocity (PGV) and displacement (PGD), response spectral acceleration and smoothed Fourier spectrum averaged for periods between 0.1 and 10 s, energy duration 5%-75% and cumulative kinetic energy. The final GOF score is defined as GOF average (from 0 to 100) of the equally-weighted abovementioned metrics. The GOF score is reported for each station and each component. More discussion on GOF results will be provided later in this section. Both the observed and simulated waveforms are band-pass filtered between 0.1 and 10 Hz.

Table 1. Strong-motion stations considered in this study. EC8 classes attributed on the basis of geological/geophysical information (Working Group ITACA, 2010) are marked by *

Code	Station name	Lon. [°E]	Lat. [°N]	R_{epi} [km]	R_{JB} [km]	EC8 class
AQG	L'Aquila-Colle Grilli	13.3370	42.3735	4.10	0.00	B
AQA	L'Aquila-F. Aterno	13.3390	42.3760	4.20	0.00	B
AQV	L'Aquila-Centro Valle	13.3439	42.3771	3.99	0.00	B
AQK	L'Aquila-Aquil Park	13.4010	42.3450	2.13	0.00	B
AQU	L'Aquila-Castello	13.4019	42.3539	2.18	0.00	B*
GSA	Gran Sasso (Assergi)	13.5194	42.4207	14.15	8.59	B
MTR	MonteReale	13.2448	42.5240	22.13	15.93	A*
FMG	Fiamignano	13.1172	42.2680	23.17	16.56	A*
ANT	Antrodoco	13.0787	42.4182	25.54	19.31	A*
CLN	Celano	13.5207	42.0852	31.79	19.95	A*
AVZ	Avezzano	13.4259	42.0275	36.15	25.14	C
CSO	Carsoli	13.0881	42.1009	36.45	31.68	A*
LSS	Leonessa	12.9689	42.5583	40.62	35.63	A*
ORC	Ortucchio	13.6424	41.9536	49.19	37.34	A*
SUL	Sulmona	13.9343	42.0895	54.29	43.35	C*
MMP	Mompeo	12.7483	42.2492	52.86	45.87	A*
SBC	Subiaco	13.1055	41.9132	53.45	46.59	A*
CHT	Chieti	14.1478	42.3698	63.47	52.17	B
SPO	Spoletto	12.7406	42.7336	67.30	62.60	A*

In general, the synthetics reproduce well the observed waveforms, despite the simplicity of the propagation models and the lack of site response for the most of the stations. The duration of the strong motion phase is well matched as well as the acceleration and velocity peak values. Concerning near fault sites (AQ_ stations), the synthetics show the characteristic velocity pulses with amplitude similar to the observed ones, at least on one component. However, an underestimation in the amplitudes and a lack of some high-frequency (> 1Hz) phases is noticed on the horizontal components (particularly on the North-South one), suggesting that more complex effects related to the presence of Aterno valley or details of source rupture model could affect the ground motion at these sites.

A comparison between observed and simulated peak acceleration (PGA) and velocity (PGV) as a function of distance for all stations reported in Table 1 is presented in Fig 4. The amplitude and distance decay of the observed peaks is generally well reproduced by the simulations. Significant differences are visible at some stations and can be ascribed to site effects not included in the modeling. For instance the large PGV value at about 50 km distance not reproduced by the model is related to

Chieti station (CHT) where large amplifications, in the mid- low-frequency range are expected (Bindi et al., 2009).

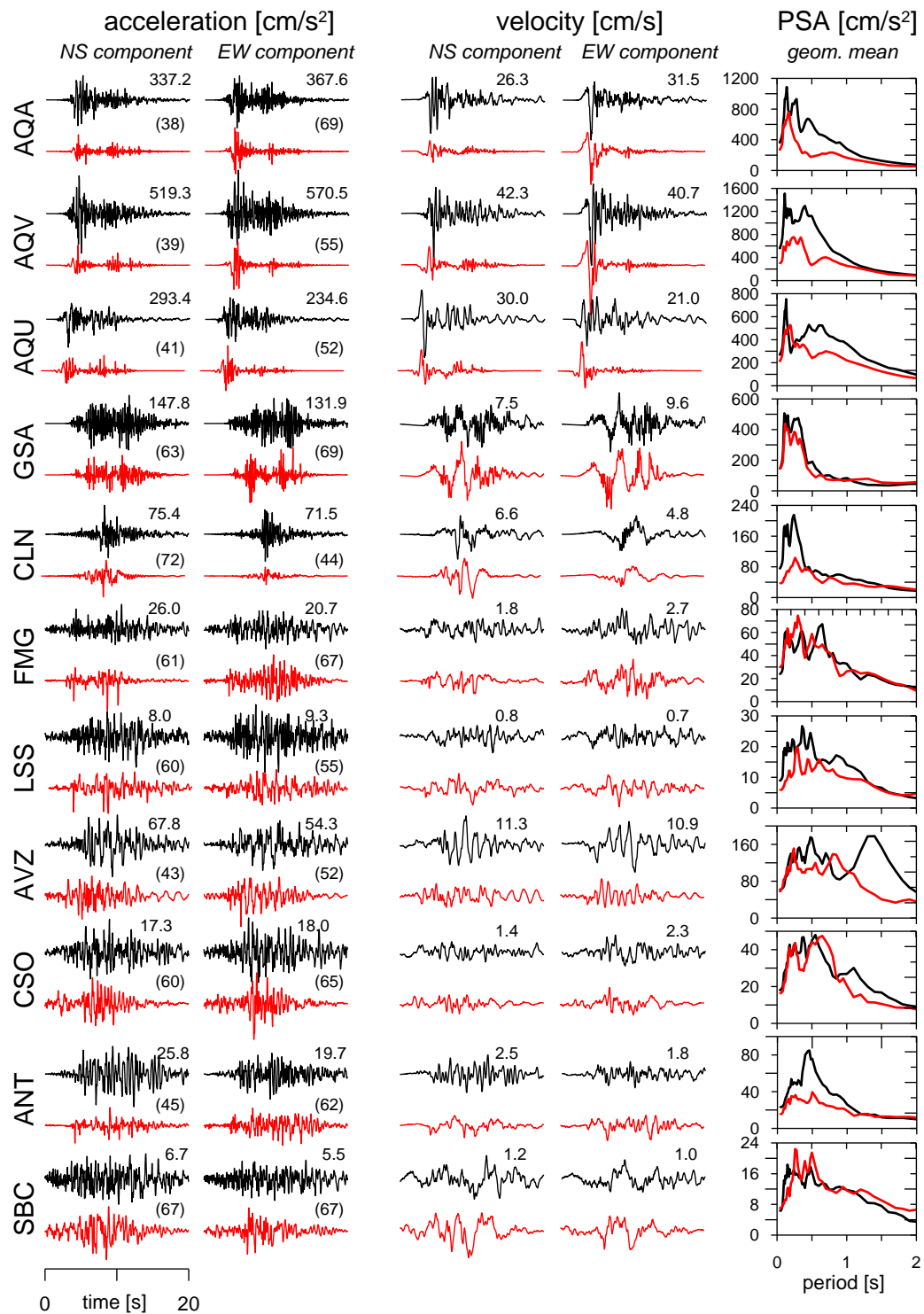


Figure 3. Comparison of recorded (black) and simulated (red) broadband ground-acceleration and velocity waveforms at 11 selected sites (indicated in Fig. 1) for the L'Aquila earthquake. North-South, East-West components are shown. The recorded and simulated motions for each station are scaled to the maximum value listed above each pair of waveforms. The numbers between brackets are the goodness-of-fit score. Waveforms are band-pass filtered between 0.1 and 10 Hz. The right-most panels show comparison of recorded (black) and simulated (red) acceleration response spectra (5% damping) for geometric mean of NS and EW components.

Beside comparisons at single stations presented in Fig. 3 and Fig.4 we also quantify the overall model bias in terms of acceleration response spectra (5% damping). In Fig. 5, the residuals are calculated as $\log_{10}(Y_{\text{obs}}/Y_{\text{sim}})$, where Y is the spectral acceleration for each period and for all stations in Table 1. The model bias is obtained by calculating the mean and standard deviation of the residuals over all stations. Fig. 5 illustrates the model bias separately for horizontal (geometric mean of NS and EW components) and vertical components. A model bias of zero indicates that the simulation, on average, matches the observed ground-motion level. A negative model bias indicates overprediction of the observations and a positive model bias indicates underprediction of the observations. The comparisons shown in Fig. 5 exhibit little systematic model bias across a wide period range. The standard deviation is about 0.2 in log10 units. There is a tendency to underestimate spectral ordinates below 1s both on horizontal and vertical components that can be ascribed to the lack of site-specific amplifications at most of the far stations.

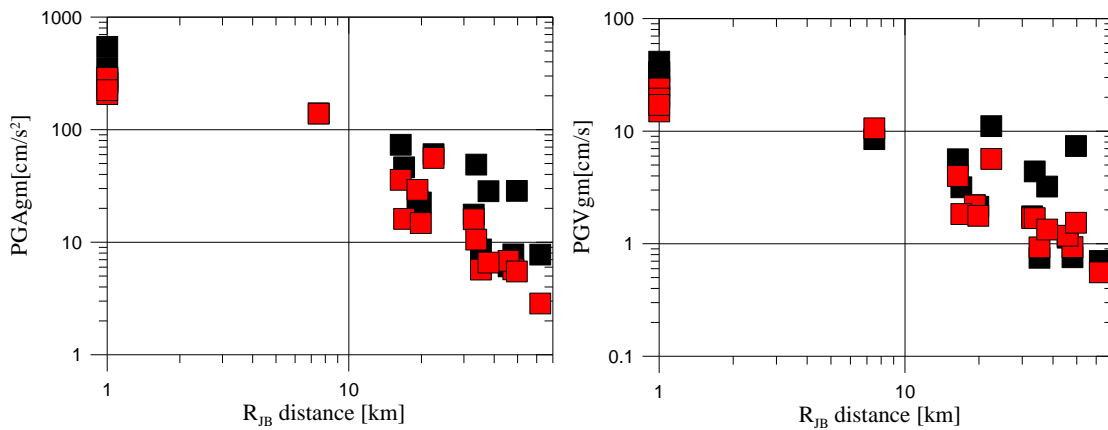


Figure 4. Comparison of recorded (black) and simulated (red) peak ground acceleration (PGA) and velocity (PGV) for geometric mean of NS and EW components as a function of Joyner-Boore distance (R_{JB}). Note that points with $R_{JB}=0$ are plotted at 1 km.

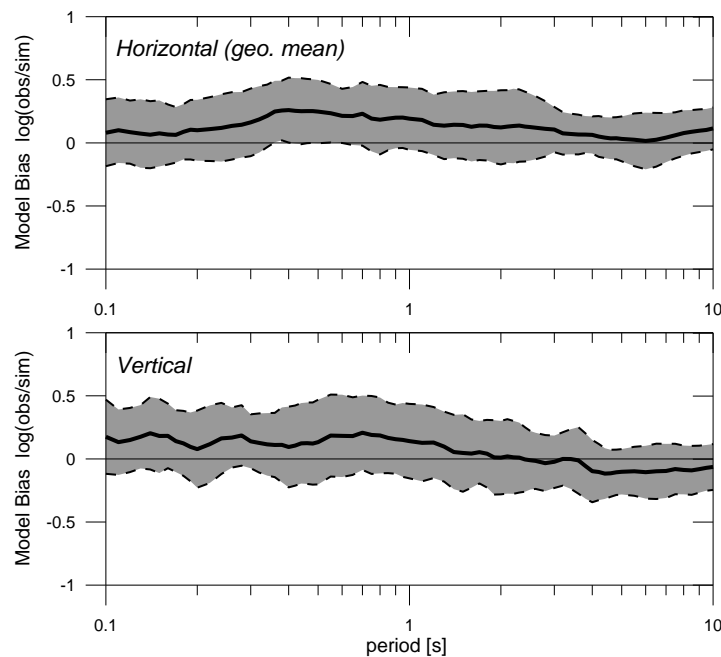


Figure 5. Model bias (thick line) and standard deviation (shaded region) for 5% damped spectral acceleration using 19 sites reported in Table 1.

Fig. 6 shows the GOF scores distribution, as defined above, for selected stations (same stations presented in Fig. 3). For each station, the distribution of GOF scores for different ground motion parameters is represented by box plots (see figure caption). Moreover, the average GOF obtained over all the considered stations is shown by the gray box. According to Olsen and Mayhew (2010) a GOF of 80–100 corresponds to an excellent fit, of 65–80 to a very good fit, of 45–65 to a fair fit, and of 35–45 to a poor fit. On average we obtain from fair to very good fits confirming the validity of the adopted source and wave propagation models.

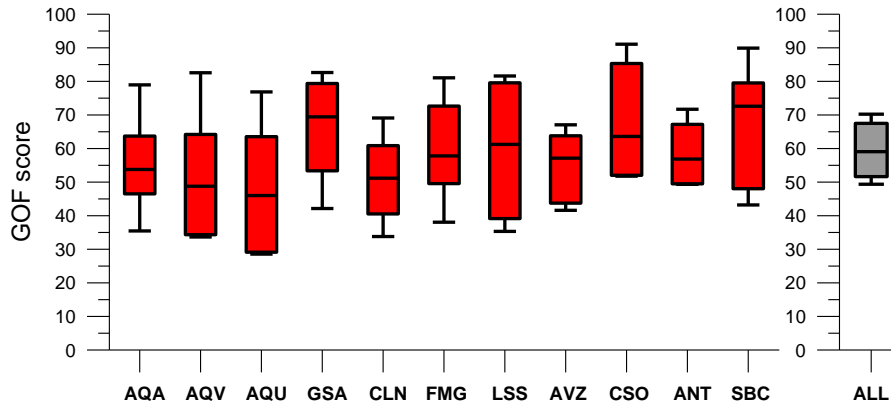


Figure 6. Goodness-of-fit (GOF) values for selected stations (red diagrams) computed according to Olsen and Mayhew (2010). The overall GOF is showed by the gray diagram. Each box represents the distribution of GOF scores for PGA, PGV, PGD, response spectral acceleration and smoothed Fourier spectrum (0.1 and 10s), energy duration 5%-75% and cumulative kinetic energy (see main text). The boxes encloses 50% of the values distribution, the upper and lower line limits are the maximum and minimum values, respectively, and the horizontal segment within each box is the 50 percentile of the distribution.

4. SHAKING SCENARIOS AND COMPARISON WITH GMPES

The proposed and validated model is adopted to calculate the bedrock ground motion (0.1-10 Hz) on a grid of points in the epicentral area in order to evaluate the motion where recording sites are not available. We consider 183 grid points up to a distance of 50 km from the fault. The inter-station distance is about 2.5 km for sites above the fault and 5 km for more distant sites. As discussed in Ameri et al. (2012), the modelling results suggested that the cross-over frequency band, dividing the integral and composite calculations, is larger for the very near-fault sites (AQ_) and smaller for other stations (see Ameri et al., 2012). Based on these findings we use the 1.5-2.0 Hz cross-over band for grid points located above the fault (i.e., within its surface projection) and the 0.3-0.6 Hz band for the other ones.

Fig. 7 shows PGA and PGV maps for the maximum of NS and EW components. The regions of maximum PGA and PGV, about 450 cm/s^2 and 50 cm/s , respectively, occur on the hanging-wall, close to the epicentre but shifted toward the shallower part of the fault. The distributions of the PGA and PGV are elongated toward south-east and this effect is more evident for PGV. In particular, PGA distribution attenuates more regularly with distance and the maxima roughly correspond to the location of the main slip asperities. On the other hand, PGV is clearly much more influenced by rupture directivity effect with maxima up-dip of the hypocenter and close to the south-eastern termination of the fault.

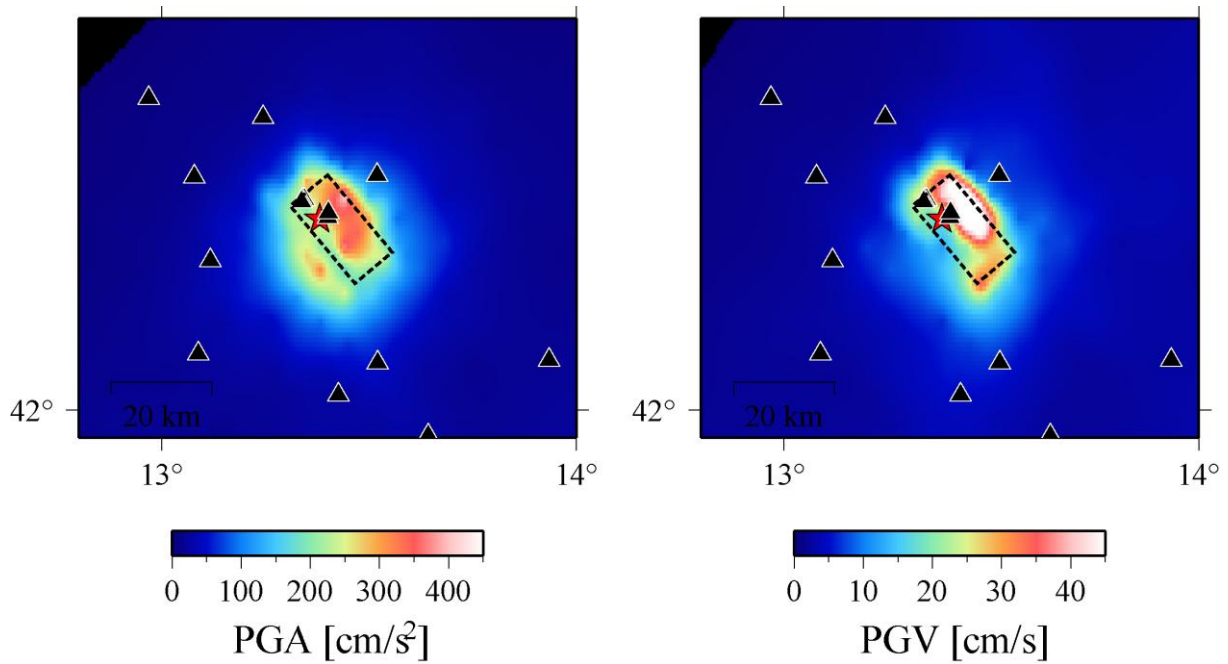


Figure 7. Simulates PGA and PGV maps (maximum of NW and EW components) for the L'Aquila earthquake. The earthquake epicenter and the surface projection of the rupture plane are indicated by the red star and the dashed rectangle, respectively

Finally, we compare the synthetic peak values simulated at the 183 sites with those estimated by empirical GMPEs for Italy and Europe (Bindi et al., 2011, Akkar and Bommer, 2010) for rock site condition (or EC8 class A sites). Fig. 8 shows that the simulated values agree with empirical ones up to roughly 5-10 km from the fault. At larger distances the synthetic values show a faster decay, especially for PGA, in general agreement with observed values during the earthquake (blue squares). The simulated ground motion variability (scatter) is larger at the shortest distances and of the same order of the standard deviation reported for the two empirical models.

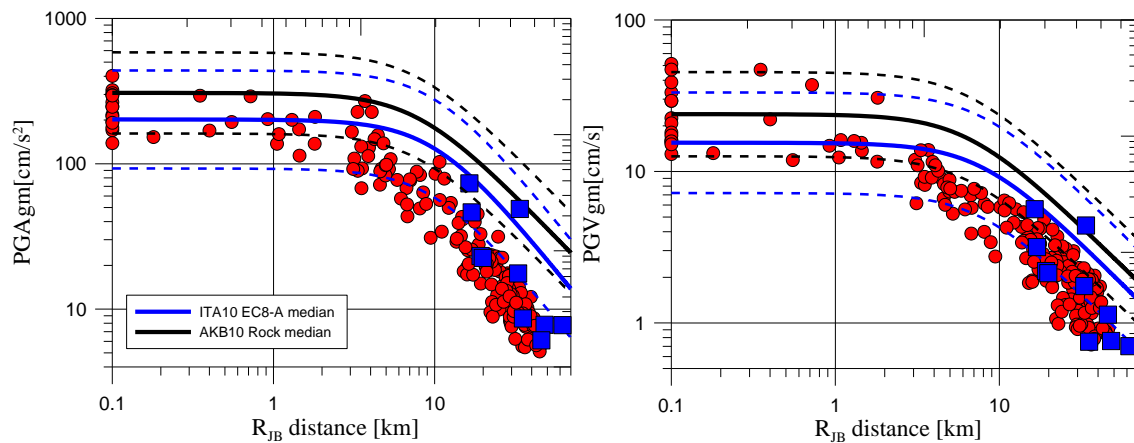


Figure 8. Comparison of simulated PGA(left) and PGV (right), red symbols, at 183 virtual sites within 50 km from the fault with empirical GMPEs for geometric mean of horizontal components. The ITA10 (Bindi et al., 2011) and AKB10 (Akkar and Bommer 2010) GMPEs are considered. Median predictions and ± 1 sigma intervals are shown by continuous and dashed lines respectively. The observed peak values at EC8 class A sites are also plotted (blue squares).

5. CONCLUSIONS

We presented the results of broadband ground-motion simulations for the 6 April 2009 (M_w 6.3) L'Aquila, central Italy, earthquake. The event has been recorded by several digital stations of the Italian Strong-Motion Network representing a unique dataset in Italy in terms of number and quality of records, azimuthal coverage and presence of near-fault recordings.

We modelled the strong-motion records of the L'Aquila earthquake over the entire frequency band of engineering concern (0.1 - 10 Hz) using a kinematic rupture model whose main features were constrained by source inversion of low-frequency (< 0.2 Hz) accelerometric records from a previous study. We utilized a hybrid integral-composite approach based on a k-square kinematic rupture model, combining low-frequency coherent and high-frequency incoherent source radiation and providing omega-squared source spectral decay.

The synthetic seismograms match well the observed waveforms both in terms of acceleration and velocity. The quality of fit was evaluated through a quantitative goodness-of-fit criteria, applied on different metrics selected from peak and integral ground parameters.

The overall results indicate that although the local site effects are important to determine the shaking at some sites, the spatial broadband ground-motion variability, both in frequency and time domain, in the epicentral area is to large extent controlled by the rupture kinematics. The validated model was then used to simulate ground-motion maps in the study area for bedrock site condition. The maps allowed us to study the spatial distribution of ground-motion parameters and to evaluate the seismic shaking in areas with absence of recording stations. We found that maximum shaking occurred on the hanging-wall side, close to the epicentre but shifted toward the shallower part of the fault. This feature is more evident for PGV and can be related to the up-dip directivity of the rupture model. Interestingly, the PGV map is in agreement with the regional pattern of the macroseismic intensities, characterized by an asymmetric shape, with the most damaged area ($I \geq 7.5$ MCS degree) extended for about 20 km and elongated in NW-SE direction (Ameri et al. 2011).

The decay of the observed amplitudes for rock sites (EC8 class A) is better described by the simulated values than by the median estimates from the selected GMPEs, at least over the distance range considered in our modeling. This comparison indicates that the ground motion in the epicentral area of L'Aquila earthquake attenuates faster than what prescribed by the European and Italian GMPEs

The model proposed for L'Aquila earthquake produces ground motion variability comparable to that of the GMPEs within 20 km from the epicentre in correspondence of the surface projection of the fault, while at larger distances the scattering is lower.

These results suggest that, in the epicentral area, the ground motion variability is mainly controlled by the source mechanism, while far from fault, other factors such as site and propagation effects, become more significant.

ACKNOWLEDGEMENT

We Acknowledge the Financial support from Project RS1 (ReLUIS-DPC 2010–2013), NERA 262330, GACR 210/11/0854, MSM0021620860 .

REFERENCES

- Akkar, S., and J. J. Bommer (2010). Empirical equations for the prediction of PGA, PGV and spectral accelerations in Europe, the Mediterranean region, and the Middle East, *Seismol. Res. Lett.* **81**, 195–206.
- Ameri G., Massa M., Bindi D., D'Alema E., Gorini A., Luzi L., Marzorati S., Pacor F., Paolucci R., Puglia R. and C. Smerzini (2009). The 6 April 2009, M_w 6.3, L'Aquila (Central Italy) earthquake: strong-motion observations. *Seismol. Res. Lett.*, **80**, 951-966.
- Ameri G., Bindi D. Pacor F. and F. Galadini (2011) The 6 April 2009, M_w 6.3, L'Aquila (Central Italy) earthquake: finite-fault effects on intensity data, *Geophys. J. Int.*, **186**, 2, 837-851.
- Ameri, G., F. Gallovič, and F. Pacor (2012), Complexity of the M_w 6.3 2009 L'Aquila (central Italy) earthquake: 2. Broadband strong motion modeling, *J. Geophys. Res.*, **117**, B04308, doi:10.1029/2011JB008729.
- Anderson, J. G., and S. E. Hough (1984). A model for the shape of the Fourier amplitude spectrum of acceleration at high frequencies, *Bull. Seismol. Soc. Am.* **74**, 1969–1993.

- Bianchi, I., C. Chiarabba, and N. Piana Agostinetti (2010), Control of the 2009 L'Aquila earthquake, central Italy, by a high-velocity structure: A receiver function study, *J. Geophys. Res.*, **115**, B12326, doi: 10.1029/2009JB007087.
- Bindi, D., R. R. Castro, G. Franceschina, L. Luzi, and F. Pacor (2004). The 1997–1998 Umbria-Marche sequence (central Italy): source, path, and site effects estimated from strong motion data recorded in the epicentral area, *J. Geophys. Res.* **109**, B04312, doi 10.1029/2003JB002857.
- Bindi D., Pacor F., Luzi L., Massa M., Ameri G. (2009). The M_w 6.3, 2009 L'Aquila earthquake: source, path and site effects from spectral analysis of strong motion data. *Geophys. J. Int.* **179**:1573–1579. doi:10.1111/j.1365-246X.2009.04392.x
- Bindi D., Pacor F., Luzi L., Puglia R., Massa M., Ameri G., Paolucci R. (2011). Ground motion prediction equations derived from the Italian strong motion data base. *Bull Earth Eng.*, **9**, 6, 1899-1920.
- Bouchon, M. (1981), A simple method to calculate Green's functions for elastic layered media, *Bull. Seism. Soc. Am.* **71**, 959-971.
- CEN, Comité Européen de Normalisation (2004). Eurocode 8: Design of Structures for Earthquake Resistance—Part 1: General Rules, Seismic Actions and Rules for Buildings, Brussels: Comité Européen de Normalisation.
- Chiarabba C, Amato A, Anselmi M, Baccheschi P, Bianchi I, Cattaneo M, Cecere G, Chiaraluce L, Ciaccio MG, De Gori P, De Luca G, Di Bona M, Di Stefano R, Faenza L, Govoni A, Improta L, Lucente FP, Marchetti A, Margheriti L, Mele F, Michelini A, Monachesi G, Moretti M, Pastori M, Piana Agostinetti N, Piccinini D, Roselli P, Seccia D, Valoroso L (2009) The 2009 L'Aquila (central Italy) M_w 6.3 earthquake: main shock and aftershocks. *Geophys Res Lett.*, **36**:L18308. doi:10.1029/2009GL039627
- Cirella, A., A. Piatanesi, M. Cocco, E. Tinti, L. Scognamiglio, A. Michelini, A. Lomax, and E. Boschi (2009), Rupture history of the 2009 LAquila (Italy) earthquake from non-linear joint inversion of strong motion and GPS data, *Geophys. Res. Lett.*, **36**, L19304.
- Di Capua G., G. Lanzo, V. Pessina, S. Peppoloni and G. Scasserra (2011) The recording stations of the Italian strong motion network: geological information and site classification, *Bull. Earthq. Eng.*, **9**, 6, 1779-1796.
- Gallovič, F., and J. Brokešová (2007). Hybrid k-squared source model for strong ground motion simulations: Introduction, *Phys. Earth Planet. In.* **160**, 34–50.
- Gallovič, F., Zahradník, J. (2011). Complexity of the $M_6.3$ 2009 L'Aquila (central Italy) earthquake: 1. Multiple finite-extent source inversion, *J. Geophys. Res.*, **117**, B04307, doi:10.1029/2011JB008709
- Herrero, A., and P. Bernard (1994). A kinematic self-similar rupture process for earthquakes, *Bull. Seismol. Soc. Am.* **84**, 1216–1228.
- Olsen, K.B., and J.E. Mayhew (2010). Goodness-of-fit Criteria for Broadband Synthetic Seismograms, With Application to the 2008 M_w 5.4 Chino Hills, CA, Earthquake, *Seism. Res. Lett.* **81**, 715-723
- NTC08, Norme Tecniche per le Costruzioni (2008). DM 140108, Ministero delle Infrastrutture, Roma, Gazzetta Ufficiale, http://www.cslp.it/cslp/index.php?option=com_content&task=view&id=66&Itemid=20 (in Italian). Last accessed January 2011.
- S4 Project –Deliverable D4 (2009). Progress report on the ongoing activity for constructing a catalogue of geological/geotechnical information at accelerometer stations. http://esse4.mi.ingv.it/images/stories/deliverable_d4.pdf .Last accessed June 2011
- Working Group ITACA (2010). Data base of the Italian strong motion records. <http://itaca.mi.ingv.it/ItacaNet/>. Last accessed on July 2011